Metamaterial-based lossy anisotropic epsilon-near-zero medium for energy collimation

Nian-Hai Shen,[1,*] Peng Zhang,[1] Thomas Koschny,[1] and Costas M. Soukoulis[1,2]

[1]*Ames Laboratory, U.S. Department of Energy and Department of Physics and Astronomy, Iowa State University, Ames, Iowa 50011, USA*

[2]*Institute of Electronic Structure and Laser, FORTH, 71110 Heraklion, Crete, Greece*

(Received 22 February 2016; revised manuscript received 20 May 2016; published 8 June 2016)

A lossy anisotropic epsilon-near-zero (ENZ) medium may lead to a counterintuitive phenomenon of omnidirectional bending-to-normal refraction [S. Feng, Phys. Rev. Lett. **108**, 193904 (2012)], which offers a fabulous strategy for energy collimation and energy harvesting. Here, in the scope of effective medium theory, we systematically investigate two simple metamaterial configurations, i.e., metal-dielectric-layered structures and the wire medium, to explore the possibility of fulfilling the conditions of such an anisotropic lossy ENZ medium by playing with materials' parameters. Both realistic metamaterial structures and their effective medium equivalences have been numerically simulated, and the results are in excellent agreement with each other. Our study provides clear guidance and therefore paves the way towards the search for proper designs of anisotropic metamaterials for a decent effect of energy collimation and wave-front manipulation.

DOI: 10.1103/PhysRevB.93.245118

I. INTRODUCTION

Metamaterials with building blocks artificially structured at a subwavelength scale have been a paradigm for manipulating propagation of waves and engineering electromagnetic space [1–4]. Besides the most well-known negative refraction [5,6], superresolution imaging [7–10], optical cloaking [11–14]. and metasurfaces [15–17], the powerful concept of metamaterials also boosted the realization of a zero-index medium [18–20] [ε-near-zero (ENZ) or μ-near-zero (MNZ) or both], which leads to many fascinating properties. including directive emission [21,22], light squeezing [23,24], scattering manipulation [25–28], etc. Generally, intrinsic loss is a hinder in metamaterials [1,29], which limits and challenges most proposed applications, and thus gain-assisted metamaterials were proposed and have attracted extensive studies [30–32]. The only exception previously found with respect to the loss in metamaterials is the perfect absorber, where loss is favored [33]. Recently, Feng revealed a counterintuitive phenomenon, i.e., the so-called anti-Snell's law, with a loss-assisted anisotropic ENZ medium, where loss plays a positive role as well [34]. Such conceptual lossy anisotropic materials were proposed to have important applications in beam collimation and energy harvesting, a different strategy than some previous studied lossless or low-loss extremely anisotropic materials [35–39]. Even though there have been several metamaterial structures tested numerically [40] and experimentally [41] for the loss-induced transmission enhancement, so far it still lacks clear guidance on practical constructions for such lossy anisotropic materials. In the current work, we systematically explore the possibilities of fulfilling the conditions of a lossy anisotropic ENZ medium by means of two simple metamaterial structures, i.e., metal-dielectric-layered stacks and the wire medium. We successfully demonstrate the effect of beam collimation with our practical designs, and our investigation enlightens the search for proper materials to build lossy anisotropic ENZ metamaterial structures or devices for beam steering and energy harvesting.

II. RESULTS AND DISCUSSIONS

First, we would like to revisit such a special category of lossy anisotropic materials by the way of the equifrequency contour (EFC). For simplicity, we can take nonmagnetic materials under consideration in the present work, and the corresponding permittivity tensor $\bar{\bar{\varepsilon}}$ is expressed in the following form under the principal coordinate system (x,y,z):

$$\bar{\bar{\varepsilon}} = \begin{bmatrix} \varepsilon_x & 0 & 0 \\ 0 & \varepsilon_y & 0 \\ 0 & 0 & \varepsilon_z \end{bmatrix}, \tag{1}$$

where material parameters ε_x, ε_y, and ε_z may be complex due to the intrinsic loss of the material. In principle, in k_x-k_z space, both k_x and k_z can be complex for lossy anisotropic materials. However, for simplicity, here we only consider the space with real k_x since in most cases, the electromagnetic (EM) waves impinge the materials from vacuum with real parallel wave vector k_x preserved. Therefore, we can get the following expressions of EFCs for TM-polarized waves in the form of Re$[k_z]$ and Im$[k_z]$, respectively:

$$\left(\frac{k_z^{\mathrm{R}}}{k_0}\right)^2 = \frac{1}{2}\left[\varepsilon_x^{\mathrm{R}} - \frac{1}{|\varepsilon_z|^2}\left(\varepsilon_x^{\mathrm{R}}\varepsilon_z^{\mathrm{R}} + \varepsilon_x^{\mathrm{I}}\varepsilon_z^{\mathrm{I}}\right)\left(\frac{k_x}{k_0}\right)^2 + |\varepsilon_x|\sqrt{1 + \frac{1}{|\varepsilon_z|^2}\left(\frac{k_x}{k_0}\right)^4 - 2\frac{\varepsilon_z^{\mathrm{R}}}{|\varepsilon_z|^2}\left(\frac{k_x}{k_0}\right)^2}\right], \tag{2}$$

$$\left(\frac{k_z^{\mathrm{I}}}{k_0}\right)^2 = \frac{1}{2}\left[-\varepsilon_x^{\mathrm{R}} + \frac{1}{|\varepsilon_z|^2}\left(\varepsilon_x^{\mathrm{R}}\varepsilon_z^{\mathrm{R}} + \varepsilon_x^{\mathrm{I}}\varepsilon_z^{\mathrm{I}}\right)\left(\frac{k_x}{k_0}\right)^2 + |\varepsilon_x|\sqrt{1 + \frac{1}{|\varepsilon_z|^2}\left(\frac{k_x}{k_0}\right)^4 - 2\frac{\varepsilon_z^{\mathrm{R}}}{|\varepsilon_z|^2}\left(\frac{k_x}{k_0}\right)^2}\right]. \tag{3}$$

Considering the special category of lossy anisotropic materials, which possess $\varepsilon_z^{\mathrm{R}} \to 0$ and $\varepsilon_z^{\mathrm{I}} \to \infty$, Eqs. (2) and (3) will degenerate to

$$\left(\frac{k_z^{\mathrm{R}}}{k_0}\right)^2 = \frac{1}{2}\left(\varepsilon_x^{\mathrm{R}} + |\varepsilon_x|\right) \tag{4}$$

*nhshen@ameslab.gov

 ©2016 American Physical Society

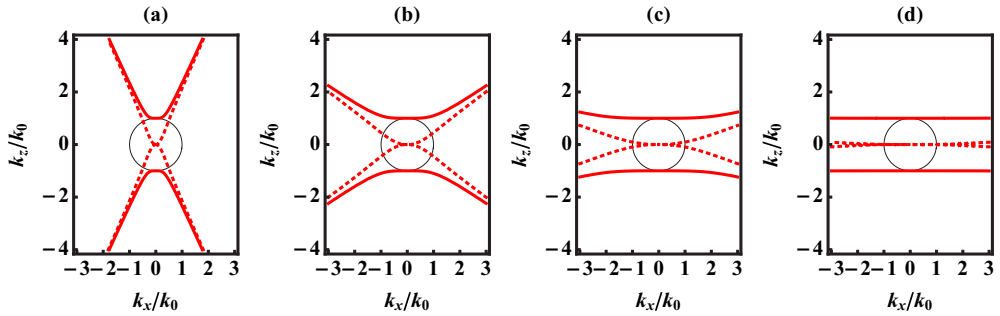

FIG. 1. Equifrequency contours of $\mathrm{Re}[k_z]/k_0$ (thick solid curve) and $\mathrm{Im}[k_z]/k_0$ (thick dotted curve) with respect to k_x/k_0 for lossy anisotropic materials with $\varepsilon_x = 1$ but (a) $\varepsilon_z = 0.1i$, (b) i, (c) $5i$, and (d) $50i$. The circular EFC of vacuum (thin solid curve) is set as a reference in each plot.

and

$$\left(\frac{k_z^{\mathrm{I}}}{k_0}\right)^2 = \frac{1}{2}\left(-\varepsilon_x^{\mathrm{R}} + |\varepsilon_x|\right). \tag{5}$$

Figures 1(a)–1(d) show the EFCs of $\mathrm{Re}[k_z]/k_0$ (thick solid curve) and $\mathrm{Im}[k_z]/k_0$ (thick dotted curve) with respect to k_x/k_0 for anisotropic materials $\varepsilon_z = 0.1i$, i, $5i$, and $50i$ ($\varepsilon_x = 1$ for all cases), respectively, in comparison with the circular EFC of vacuum (thin solid curve). From Fig. 1, we find that, as $\varepsilon_z^{\mathrm{I}}$ increases, the EFC of $\mathrm{Re}[k_z]/k_0$ becomes flatter and flatter, and surprisingly, on the other hand, $\mathrm{Im}[k_z]$ gradually gets smaller. Therefore, clearly, according to Fig. 1, we can expect a low-loss beam collimation effect with such a special category of high-loss anisotropic materials, which to some extent is counterintuitive. In addition, we also find the transmission of energy for TM-polarized waves, which is expressed in the form $T^{\mathrm{TM}} = \mathrm{Re}[S_{2z}]/\mathrm{Re}[S_{2x}] = (\mathrm{Re}[k_{2z}/\varepsilon_{2x}]/\mathrm{Re}[k_{1z}/\varepsilon_1])|t^{\mathrm{TM}}|^2$, can remain at over 50% even for an 80° angle of incidence at the interface of air and lossy anisotropic ENZ materials. Therefore, the introduction of these anisotropic materials will lead to an omnidirectional high-efficiency energy collimation effect, which may be greatly beneficial to the field of energy harvesting and storage. Based on the brief discussion above, a large $\mathrm{Im}[\varepsilon_z]$ is desirable to achieve a satisfying beam collimation effect, and we hope the value of $\mathrm{Im}[\varepsilon_x]$ is as small as possible to prevent severe decay of the collimated beam inside the anisotropic material.

In the present work, we focus on the exploration of possible configurations to achieve the aforementioned lossy anisotropic ENZ materials. Figure 2 shows the schematic of the metal-dielectric-layered structure and wire medium under investigation, in both so-called parallel [Figs. 2(a) and 2(c)] and perpendicular [Figs. 2(b) and 2(d)] configurations.

A. Metal-dielectric-layered structure

For the metal-dielectric-layered structure under parallel configuration as shown in Fig. 1(a), Maxwell-Garnett theory [42] gives

$$\varepsilon_z = \varepsilon_\perp = \frac{1}{f/\varepsilon_{\mathrm{M}} + (1-f)/\varepsilon_{\mathrm{D}}} \tag{6}$$

and

$$\varepsilon_x = \varepsilon_{//} = f\varepsilon_{\mathrm{M}} + (1-f)\varepsilon_{\mathrm{D}}, \tag{7}$$

where $\perp$ ($//$) means the direction perpendicular (parallel) to the metal/dielectric layers, f is the filling ratio of metal layers over the period, and ε_{M} and ε_{D} represent permittivities of metal and dielectric materials, respectively. For further derivations, ε_{M} can be written in the form with separated real and imaginary parts as $\varepsilon_{\mathrm{M}} = \varepsilon_{\mathrm{M}}^{\mathrm{R}} + i\varepsilon_{\mathrm{M}}^{\mathrm{I}}$, and so can ε_{D}, with $\varepsilon_{\mathrm{D}} = \varepsilon_{\mathrm{D}}^{\mathrm{R}} + i\varepsilon_{\mathrm{D}}^{\mathrm{I}}$. Therefore, from Eq. (6), we can get the expressions of the real and imaginary parts of ε_z as follows:

$$\mathrm{Re}[\varepsilon_z] = \frac{f\varepsilon_{\mathrm{M}}^{\mathrm{R}}|\varepsilon_{\mathrm{D}}|^2 + (1-f)\varepsilon_{\mathrm{D}}^{\mathrm{R}}|\varepsilon_{\mathrm{M}}|^2}{f^2|\varepsilon_{\mathrm{D}}|^2 + (1-f)^2|\varepsilon_{\mathrm{M}}|^2 + 2f(1-f)\left(\varepsilon_{\mathrm{M}}^{\mathrm{R}}\varepsilon_{\mathrm{D}}^{\mathrm{R}} + \varepsilon_{\mathrm{M}}^{\mathrm{I}}\varepsilon_{\mathrm{D}}^{\mathrm{I}}\right)}, \tag{8}$$

$$\mathrm{Im}[\varepsilon_z] = \frac{f\varepsilon_{\mathrm{M}}^{\mathrm{I}}|\varepsilon_{\mathrm{D}}|^2 + (1-f)\varepsilon_{\mathrm{D}}^{\mathrm{I}}|\varepsilon_{\mathrm{M}}|^2}{f^2|\varepsilon_{\mathrm{D}}|^2 + (1-f)^2|\varepsilon_{\mathrm{M}}|^2 + 2f(1-f)\left(\varepsilon_{\mathrm{M}}^{\mathrm{R}}\varepsilon_{\mathrm{D}}^{\mathrm{R}} + \varepsilon_{\mathrm{M}}^{\mathrm{I}}\varepsilon_{\mathrm{D}}^{\mathrm{I}}\right)}. \tag{9}$$

To fulfill the condition of $\varepsilon_z = 0$, the filling ratio of metal layers needs to have the following value from Eq. (8):

$$f = \frac{\varepsilon_{\mathrm{D}}^{\mathrm{R}}|\varepsilon_{\mathrm{M}}|^2}{\varepsilon_{\mathrm{D}}^{\mathrm{R}}|\varepsilon_{\mathrm{M}}|^2 - \varepsilon_{\mathrm{M}}^{\mathrm{R}}|\varepsilon_{\mathrm{D}}|^2}. \tag{10}$$

By applying Eq. (10) to Eq. (9), we get $\mathrm{Im}[\varepsilon_z]$ in the form of the material parameters,

$$\mathrm{Im}[\varepsilon_z] = \frac{\varepsilon_{\mathrm{D}}^{\mathrm{R}}|\varepsilon_{\mathrm{M}}|^2 - \varepsilon_{\mathrm{M}}^{\mathrm{R}}|\varepsilon_{\mathrm{D}}|^2}{\varepsilon_{\mathrm{D}}^{\mathrm{R}}\varepsilon_{\mathrm{M}}^{\mathrm{I}} - \varepsilon_{\mathrm{M}}^{\mathrm{R}}\varepsilon_{\mathrm{D}}^{\mathrm{I}}}. \tag{11}$$

With respect to ε_x, the real and imaginary parts can be expressed respectively as follows after some algebra derivations:

$$\mathrm{Re}[\varepsilon_x] = \frac{\varepsilon_{\mathrm{D}}^{\mathrm{R}}\varepsilon_{\mathrm{M}}^{\mathrm{R}}(|\varepsilon_{\mathrm{M}}|^2 - |\varepsilon_{\mathrm{D}}|^2)}{\varepsilon_{\mathrm{D}}^{\mathrm{R}}|\varepsilon_{\mathrm{M}}|^2 - \varepsilon_{\mathrm{M}}^{\mathrm{R}}|\varepsilon_{\mathrm{D}}|^2} \tag{12}$$

and

$$\mathrm{Im}[\varepsilon_x] = \frac{\varepsilon_{\mathrm{D}}^{\mathrm{R}}\varepsilon_{\mathrm{M}}^{\mathrm{I}}|\varepsilon_{\mathrm{M}}|^2 - \varepsilon_{\mathrm{M}}^{\mathrm{R}}\varepsilon_{\mathrm{D}}^{\mathrm{I}}|\varepsilon_{\mathrm{D}}|^2}{\varepsilon_{\mathrm{D}}^{\mathrm{R}}|\varepsilon_{\mathrm{M}}|^2 - \varepsilon_{\mathrm{M}}^{\mathrm{R}}|\varepsilon_{\mathrm{D}}|^2}. \tag{13}$$

Therefore, with the choice of specific metallic and dielectric materials in the structure of Fig. 2(a), Eqs. (10)–(13) can give us the corresponding value of the filling ratio f to construct the

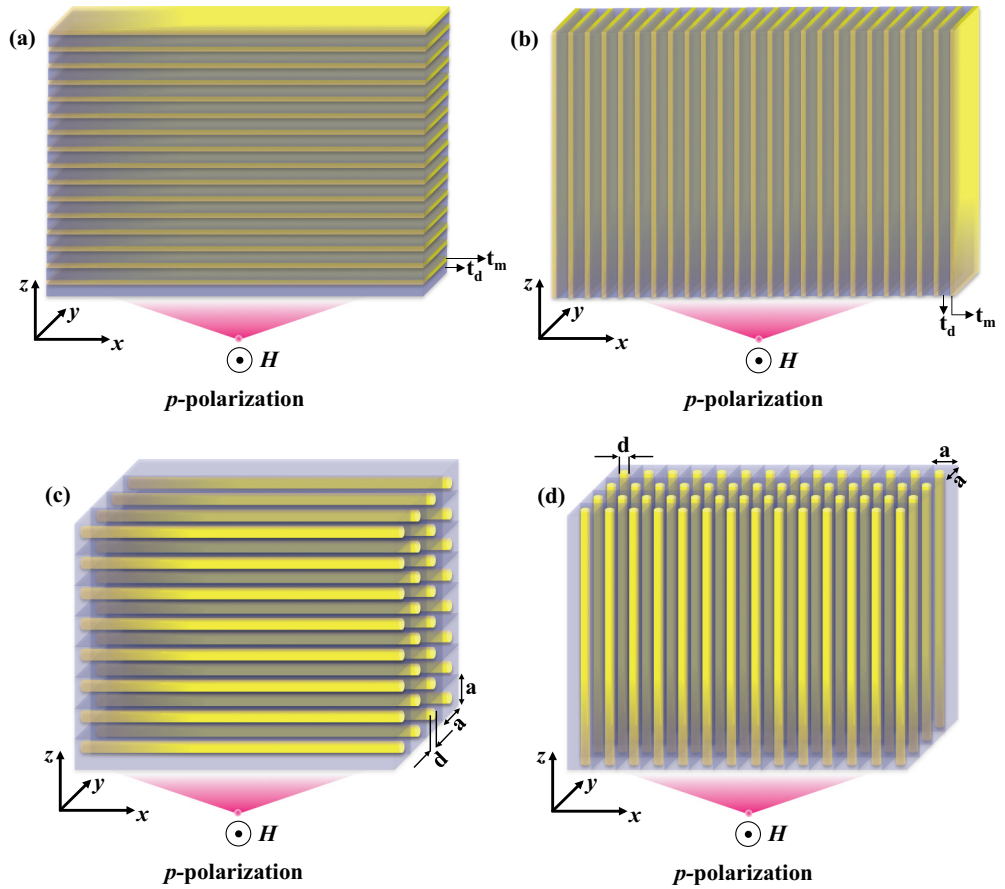

FIG. 2. Schematic of (a) and (b) metal-dielectric layered structure and (c) and (d) wire medium under parallel (left) and perpendicular (right) configurations.

lossy anisotropic ENZ material and other material parameters of the effective medium, i.e., $\mathrm{Im}[\varepsilon_z]$, $\mathrm{Re}[\varepsilon_x]$, and $\mathrm{Im}[\varepsilon_x]$. In Fig. 3, we show the results of searching for appropriate metallic materials for a zero-$\mathrm{Re}[\varepsilon_z]$ anisotropic medium with a metal-dielectric-layered structure in the parallel stack configuration [see Fig. 2(a)] for a preset dielectric material with $\varepsilon_\mathrm{D} = 12 + 0.01i$. For Figs. 3(a)–3(d), the x and y axes correspond to the change in $\mathrm{Re}[\varepsilon_\mathrm{M}]$ and $\mathrm{Im}[\varepsilon_\mathrm{M}]$, respectively, and the color map shows the values of targeted parameters. With respect to the filling ratio, we would like a moderate value to avoid too thin or too thick metal or dielectric layers, and thus, Fig. 3(a) provides clear guidance for the filling ratio. As we already pointed out above, the two most important points for achieving the high-efficiency energy collimation effect are low $\mathrm{Im}[\varepsilon_x]$ and low $\mathrm{Im}[\varepsilon_z]$ of the effective medium, which are indicated in Figs. 3(b) and 3(c), respectively. The white dashed line in Fig. 3(b) corresponds to the border with $\mathrm{Im}[\varepsilon_x] = 0.2$, and we hope the choice of the metallic material can make the value of $\mathrm{Im}[\varepsilon_x]$ settle below it to prevent dramatic decay of energy inside the anisotropic medium. On the other hand, according to Fig. 3(c), metallic materials with parameters in the bottom left are desirable to give high $\mathrm{Im}[\varepsilon_z]$. We see $\mathrm{Im}[\varepsilon_x]$ and $\mathrm{Im}[\varepsilon_z]$ do have some contradictory tendency upon changing the property of the metallic material, and therefore, we need to balance these conditions to make the choice of the metallic material accordingly. For a complete impression of the constructed effective medium, the parametric map of $\mathrm{Re}[\varepsilon_x]$ is shown in Fig. 3(d) for different metallic materials applied in the configuration.

In parallel, Fig. 4 gives the results of searching for appropriate dielectric materials to construct the desired zero-$\mathrm{Re}[\varepsilon_z]$ anisotropic medium with the configuration in Fig. 2(a), assuming the metallic material has $\varepsilon_\mathrm{M} = -5 + 0.5i$. From Fig. 4(b), it is required for us to set ε_D in the area in the bottom right corner to get low $\mathrm{Im}[\varepsilon_x]$, and Fig. 4(c) indicates high $\mathrm{Im}[\varepsilon_z]$ occurs more or less in the same area; that is, a low-loss, high-index dielectric material is highly desired in this case. On the other hand, we still need to take the filling ratio [see Fig. 4(a)] into account, so that the condition of potential fabrication is not too challenging. The color map of $\mathrm{Re}[\varepsilon_x]$ is again presented in Fig. 4(d) for complete knowledge of the constructed layered structure.

As we have seen, our theoretical analysis and numerical calculations do offer us clear guidance in selecting appropriate ingredients to construct a satisfying high-loss anisotropic ENZ medium with the metal-dielectric-layered configuration in Fig. 2(a). By searching various plasmonic materials accordingly, we find aluminum-doped zinc oxide (AZO), which has $\varepsilon_\mathrm{M} \approx -2 + 0.5i$ at free-space wavelength $\lambda = 1.5\ \mu\mathrm{m}$ [43,44], is a good candidate to serve as the metal layers here. With the dielectric $\varepsilon_\mathrm{D} = 12 + 0.01i$, we would like to perform numerical simulations for the corresponding constructed metal-dielectric-layered structure and its effective medium equivalence as well. Considering the

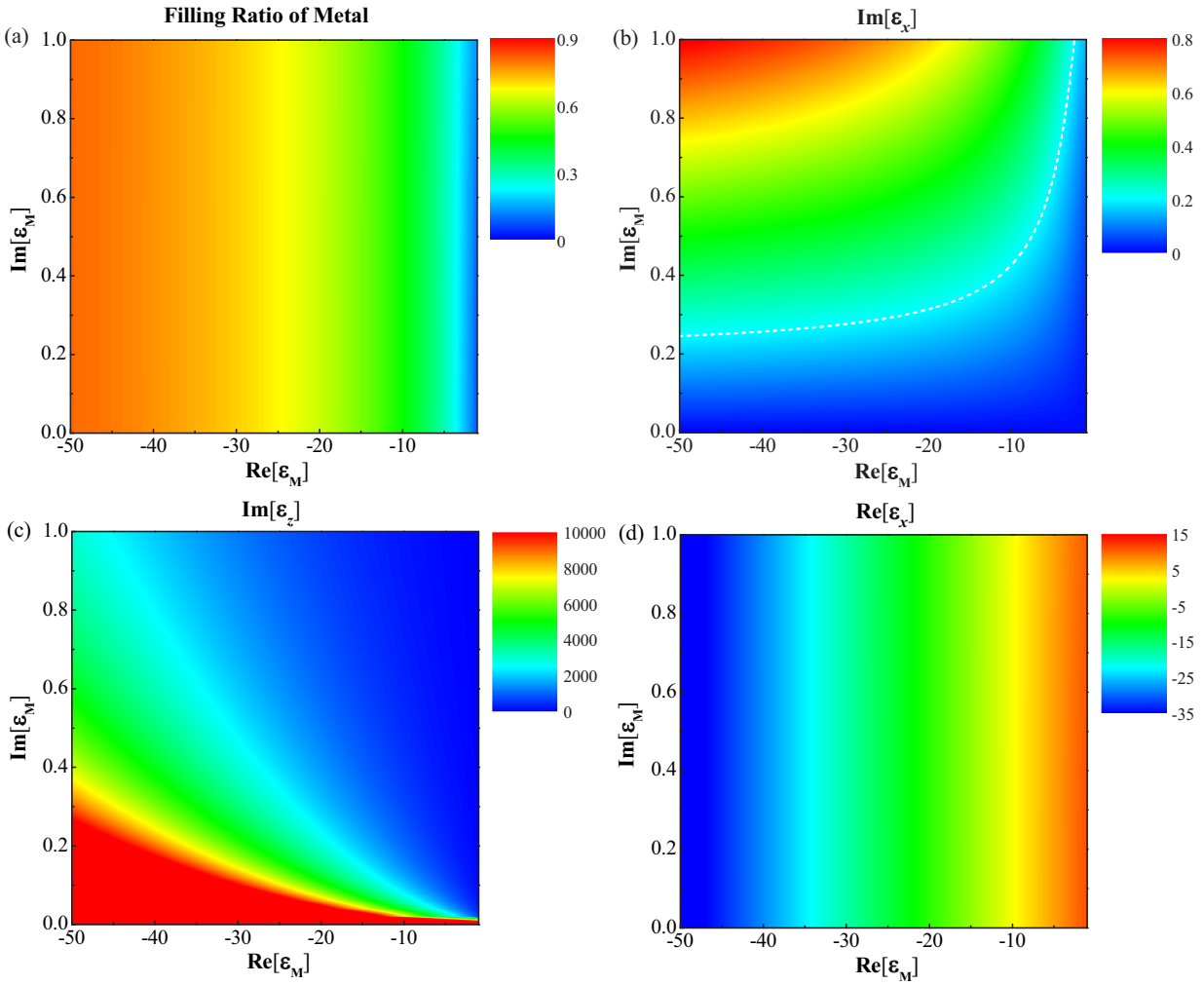

FIG. 3. The case of metal-dielectric-layered structure under configuration I with $\varepsilon_{\mathrm{D}} = 12 + 0.01i$: Dependence of (a) the filling ratio of metal for $\mathrm{Re}[\varepsilon_z] = 0$, (b) $\mathrm{Im}[\varepsilon_x]$, (c) $\mathrm{Im}[\varepsilon_z]$, and (d) $\mathrm{Re}[\varepsilon_x]$ with respect to different material parameters of the metal ε_{M}. The dashed line in (b) corresponds to $\mathrm{Im}[\varepsilon_x] = 0.2$.

chosen materials, the condition of zero $\mathrm{Re}[\varepsilon_z]$ gives the filling ratio $f = 0.15$, and the thicknesses of metallic (t_{m}) and dielectric (t_{d}) layers are set at 15 and 85 nm, respectively. The corresponding λ/t, where $t = t_{\mathrm{m}} + t_{\mathrm{d}}$ is the period of the layered structure, will be 15, and the structure thus can be well treated as an effective medium with properties described in Eqs. (6) and (7). Figure 5 shows the effect of energy collimation by setting a magnetic line source in vacuum in front of the designed metal-dielectric-layered structure in Fig. 5(b) and its effective medium equivalence in Fig. 5(a). The simulations are performed with the commercial software COMSOL MULTIPHYSICS with perfectly matched layers assigned at all the surrounding boundaries. According to Fig. 5, the beams of almost any angle of incidence are collimated inside of such an anisotropic medium with fairly low decay in the propagation. The perfect consistency in results for a realistic stacked structure and the corresponding effective medium is also an indication that the layered configuration considered here can be very well treated as an effective medium.

Similarly, we can also study the possibilities of realizing the high-loss zero-$\mathrm{Re}[\varepsilon_z]$ anisotropic medium with the other configuration of the metal-dielectric-layered structure shown in Fig. 2(b). According to the Maxwell-Garnett theory [42], we get

$$\varepsilon_z = \varepsilon_{//} = f\varepsilon_{\mathrm{M}} + (1-f)\varepsilon_{\mathrm{D}} \tag{14}$$

and

$$\varepsilon_x = \varepsilon_{\perp} = \frac{1}{f/\varepsilon_{\mathrm{M}} + (1-f)/\varepsilon_{\mathrm{D}}}. \tag{15}$$

By setting $\mathrm{Re}[\varepsilon_z] = 0$, we can easily get the simple expression for the required filling ratio of metallic layers in the form of ε_{M} and ε_{D} as follows:

$$f = \frac{\varepsilon_{\mathrm{D}}^{\mathrm{R}}}{\varepsilon_{\mathrm{D}}^{\mathrm{R}} - \varepsilon_{\mathrm{M}}^{\mathrm{R}}}. \tag{16}$$

Then, $\mathrm{Im}[\varepsilon_z]$ can also be expressed in a simple form as

$$\mathrm{Im}[\varepsilon_z] = \frac{\varepsilon_{\mathrm{D}}^{\mathrm{R}}\varepsilon_{\mathrm{M}}^{\mathrm{I}} - \varepsilon_{\mathrm{M}}^{\mathrm{R}}\varepsilon_{\mathrm{D}}^{\mathrm{I}}}{\varepsilon_{\mathrm{D}}^{\mathrm{R}} - \varepsilon_{\mathrm{M}}^{\mathrm{R}}}. \tag{17}$$

For ε_x, we can also replace f with Eq. (16) in Eq. (15) and extract $\mathrm{Im}[\varepsilon_x]$. We find that the expression for the parametric dependence of $\mathrm{Im}[\varepsilon_x]$ is fairly complicated, so the relevant

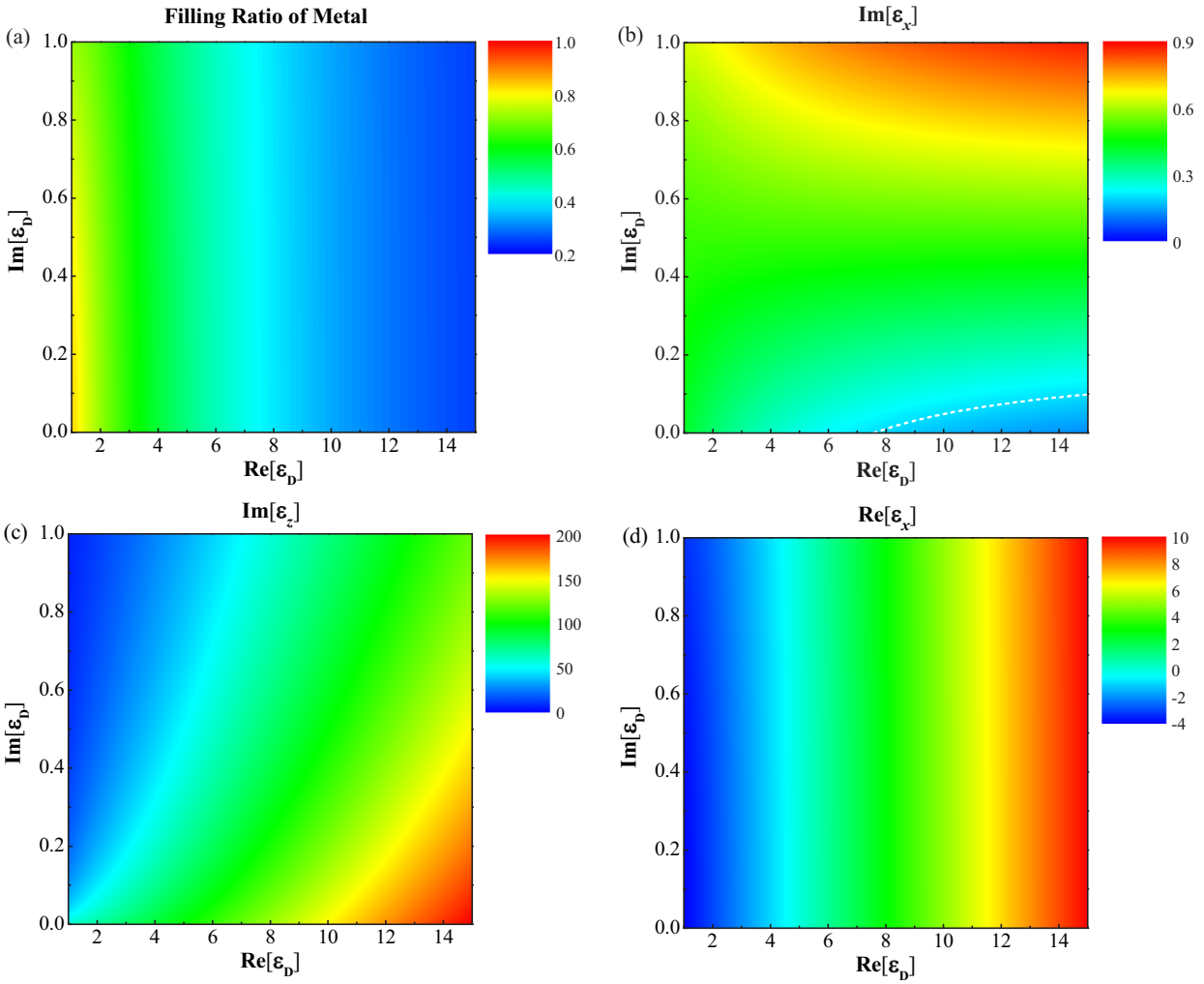

FIG. 4. The case of metal-dielectric-layered structure under configuration I with $\varepsilon_{\mathrm{M}} = -5 + 0.5i$: Dependence of (a) the filling ratio of metal for $\mathrm{Re}[\varepsilon_z] = 0$, (b) $\mathrm{Im}[\varepsilon_x]$, (c) $\mathrm{Im}[\varepsilon_z]$, and (d) $\mathrm{Re}[\varepsilon_x]$ with respect to different material parameters of the dielectric ε_{D}. The dashed line in (b) corresponds to $\mathrm{Im}[\varepsilon_x] = 0.2$.

information may be understood more intuitively through direct numerical calculations, which will be shown below.

Figures 6(a)–6(d) present the dependence of the filling ratio of the metallic layers f for $\mathrm{Re}[\varepsilon_z] = 0$, $\mathrm{Im}[\varepsilon_x]$, $\mathrm{Im}[\varepsilon_z]$, and $\mathrm{Re}[\varepsilon_x]$, respectively, on the property of the metallic material in the configuration in Fig. 2(b) for a preset dielectric material $\varepsilon_{\mathrm{D}} = 12 + 0.01i$. From Figs. 6(b) and 6(c), we can see we should choose a metallic material with both large $\mathrm{Re}[\varepsilon_{\mathrm{M}}]$ and $\mathrm{Im}[\varepsilon_{\mathrm{M}}]$ to achieve the conditions of low $\mathrm{Im}[\varepsilon_x]$ and high $\mathrm{Im}[\varepsilon_z]$ for a satisfying high-efficiency energy collimation effect. In contrast, we show, in Fig. 7, the results for the configuration in Fig. 2(b) with ε_{M} preset to be $-100 + 100i$ but with varying dielectric materials. The white dashed line in Fig. 7(b), which corresponds to $\mathrm{Im}[\varepsilon_x] = 0.2$, defines the desired area for the choice of the dielectric material for low decay of the collimated beam inside the anisotropic medium. When f and $\mathrm{Im}[\varepsilon_z]$ are also taken into account, we conclude that the bottom area is still preferred.

Indeed, Figs. 6 and 7 clearly guide us in searching for the proper ingredient, especially the metallic material to build the desired anisotropic medium using the configuration in Fig. 2(b), and accordingly, we find zirconium nitride (ZrN) with $\varepsilon_{\mathrm{M}} = -172.73 + 196.92i$ at $\lambda = 3$ μm [44] should be a good choice for metal layers here. We therefore consider the example construction in Fig. 2(b) made with ZrN and a dielectric material with $\varepsilon_{\mathrm{D}} = 10 + 0.001i$ to demonstrate the desired energy collimation effect by performing the corresponding full-wave simulations. The thicknesses of the ZrN and dielectric layers are 16.5 and 283.5 nm, respectively, and $\lambda/t \sim 10$ makes the effective medium equivalence still hold. Figure 8 shows the simulation results of the y component of the magnetic field H_y for a magnetic line source placed in the vacuum in front of the designed anisotropic medium for both the realistic metal-dielectric-layered structure [Fig. 8(b)] and its effective medium equivalence [Fig. 8(a)]. We again demonstrate the decent energy collimation for our design, which suffers from some broadening effects along the propagation inside the anisotropic medium compared to the previous parallel-stack configuration. The effective medium theory is also proved to work perfectly here through a comparison of Figs. 8(a) and 8(b), which show almost the same field distribution in both cases. Therefore, such a configuration

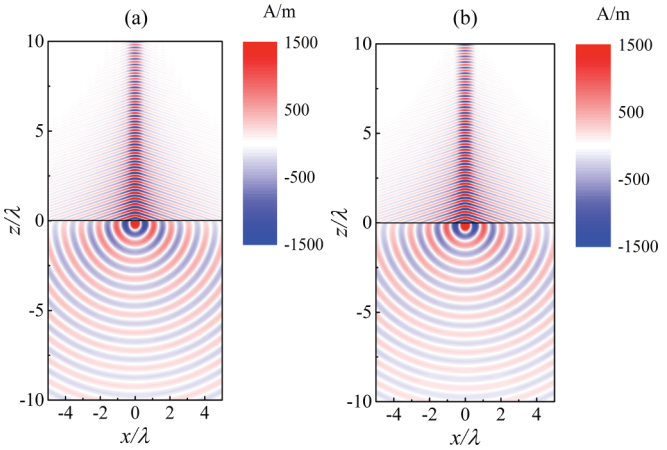

FIG. 5. y component of magnetic field, i.e., H_y for a metal-dielectric-layered structure at $\lambda = 1.5\ \mu$m under configuration I: (a) Homogeneous effective medium equivalence and (b) realistic layered structure. Metal layers are 15-nm-thick AZO with $\varepsilon_{\rm M} = -2 + 0.5i$, and dielectric layers have $\varepsilon_{\rm D} = 12 + 0.01i$ with a thickness of 85 nm.

can serve as a candidate for a practical device for energy collimation as well.

B. Wire-medium structure

The wire medium, specifically referring to metallic wires embedded in the matrix of some dielectric material here, is another popular metamaterial structure, which has been extensively studied in recent decades, both in theory and experiment [45–48]. It may also be described by the effective medium theory with the properties mathematically predicted in the form of $\varepsilon_{\rm M}$, $\varepsilon_{\rm D}$, and the filling ratio of metallic wires f. To construct the expected lossy zero-Re[ε_z] anisotropic medium with a wire medium, both the parallel and perpendicular configurations, as shown in Figs. 2(c) and 2(d), respectively, are considered and discussed in the following.

First, we would like to investigate the parallel configuration, the effective medium parameters of which can be expressed as [42]

$$\varepsilon_z = \varepsilon_\perp = \varepsilon_{\rm D}\frac{(1+f)\varepsilon_{\rm M} + (1-f)\varepsilon_{\rm D}}{(1-f)\varepsilon_{\rm M} + (1+f)\varepsilon_{\rm D}} \tag{18}$$

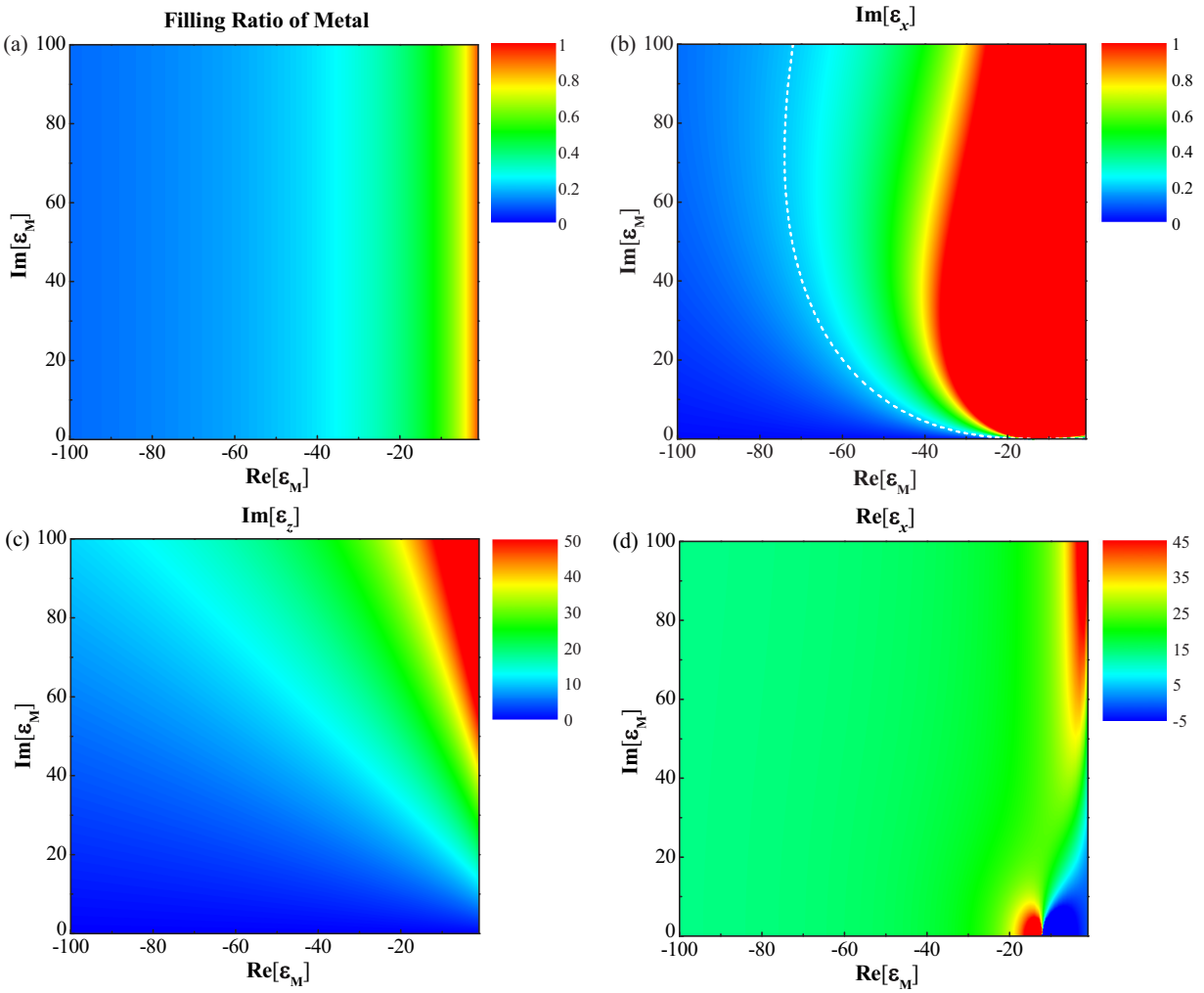

FIG. 6. The case of metal-dielectric-layered structure under configuration II with $\varepsilon_{\rm D} = 12 + 0.01i$: Dependence of (a) the filling ratio of metal for Re[ε_z] = 0, (b) Im[ε_x], (c) Im[ε_z], and (d) Re[ε_x] with respect to different material parameters of the metal $\varepsilon_{\rm M}$. The dashed line in (b) corresponds to Im[ε_x] = 0.2.

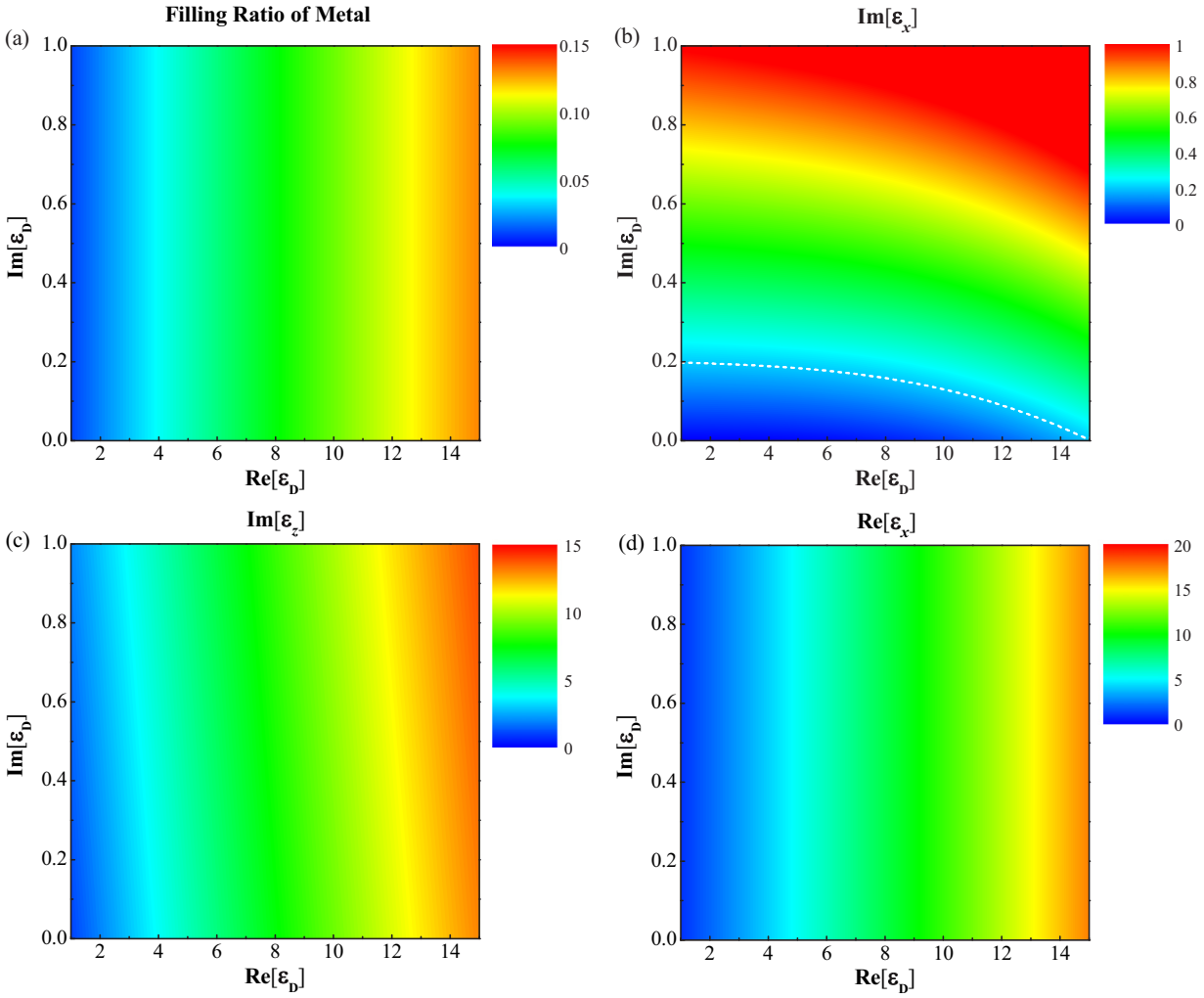

FIG. 7. The case of metal-dielectric-layered structure under configuration II with $\varepsilon_{\mathrm{M}} = -100 + 100i$: Dependence of (a) the filling ratio of metal for $\mathrm{Re}[\varepsilon_z] = 0$, (b) $\mathrm{Im}[\varepsilon_x]$, (c) $\mathrm{Im}[\varepsilon_z]$, and (d) $\mathrm{Re}[\varepsilon_x]$ with respect to different material parameters of the dielectric ε_{D}. The dashed line in (b) corresponds to $\mathrm{Im}[\varepsilon_x] = 0.2$.

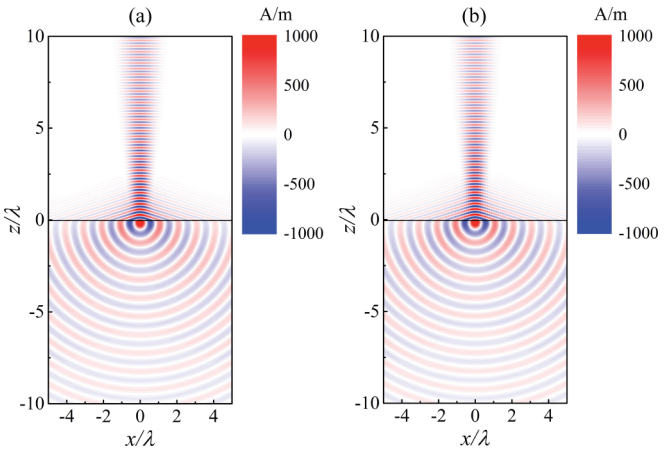

FIG. 8. y component of magnetic field, i.e., H_y for a metal-dielectric-layered structure at $\lambda = 3\ \mu$m (frequency 100 THz) under configuration II: (a) Homogeneous effective medium equivalence and (b) realistic layered structure. Metal layers are 16.5-nm-thick ZrN with $\varepsilon_{\mathrm{M}} = -172.73 + 196.92i$, and dielectric layers are 283.5 nm thick with $\varepsilon_{\mathrm{D}} = 10 + 0.001i$.

and

$$\varepsilon_x = \varepsilon_{//} = f\varepsilon_{\mathrm{M}} + (1-f)\varepsilon_{\mathrm{D}}. \tag{19}$$

Since the condition of zero $\mathrm{Re}[\varepsilon_z]$ will lead to a fairly complicated form of f and the following $\varepsilon_{x,z}$ as well, which are not intuitive, we would like to numerically search for appropriate materials to construct the desired wire medium, instead of presenting the analytical expressions.

Figure 9 shows the dependence of f, $\mathrm{Im}[\varepsilon_z]$, $\mathrm{Im}[\varepsilon_x]$, and $\mathrm{Re}[\varepsilon_x]$ on the properties of metallic wires for a preset dielectric matrix material, which has $\varepsilon_{\mathrm{D}} = 12 + 0.01i$. The metallic material with ε_{M} settled within the area of the white dashed lines (corresponding to $\mathrm{Im}[\varepsilon_x] = 0.2$) in Fig. 9(b) is preferred for relatively lower loss of the collimated EM waves in propagation in the constructed anisotropic medium. Figure 9(c) provides guidance for the choice of the metallic material leading to a better collimation effect of energy with larger $\mathrm{Im}[\varepsilon_z]$, and we find the bottom left area of ε_{M} is more desirable. On the other hand, a moderate value for the filling ratio of metallic wires needs to be taken into account as well, as shown in Fig. 9(a). We should note that ε_{M} of practical

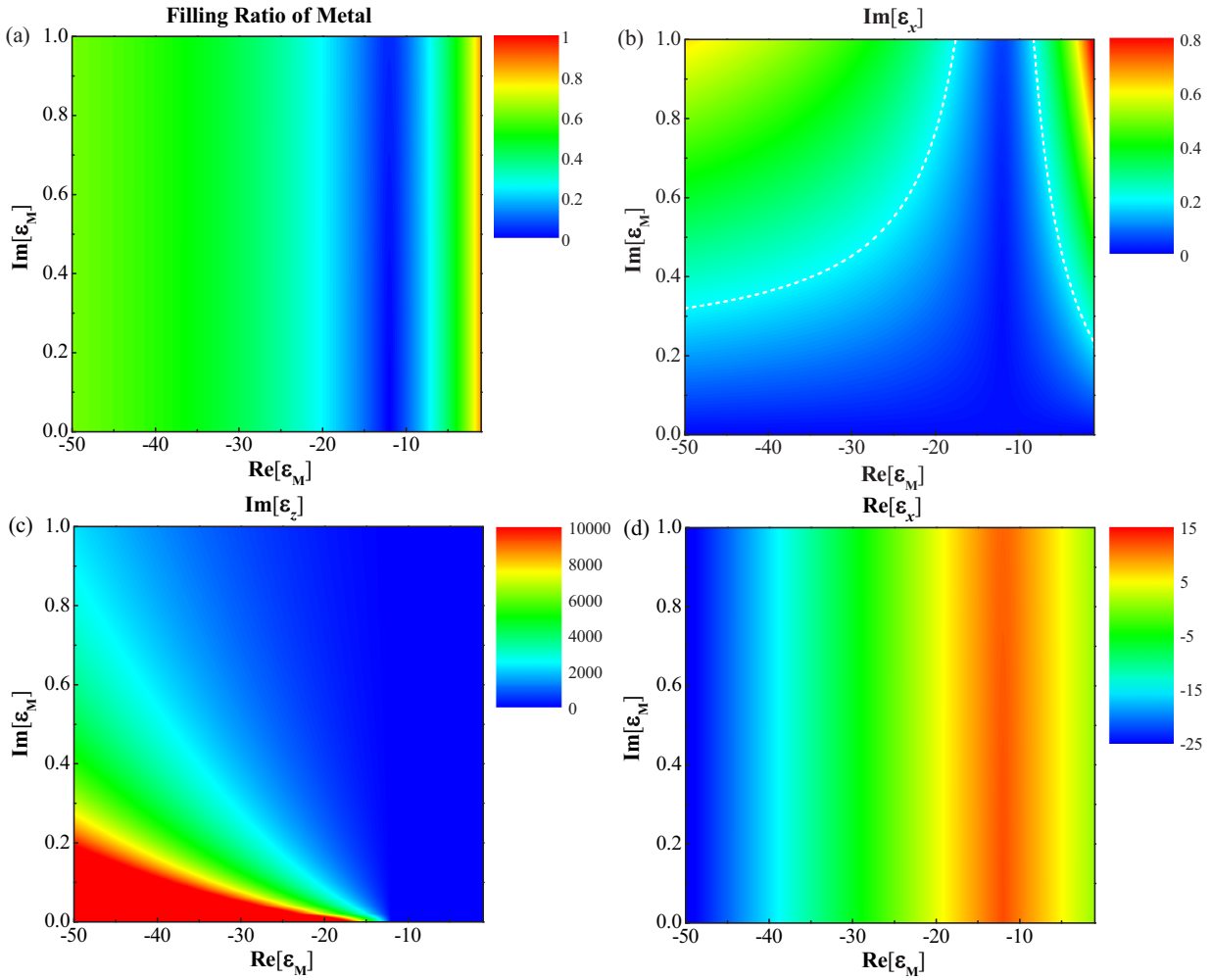

FIG. 9. The case of a wire medium under configuration I with $\varepsilon_{\mathrm{D}} = 12 + 0.01i$: Dependence of (a) the filling ratio of metal for $\mathrm{Re}[\varepsilon_z] = 0$, (b) $\mathrm{Im}[\varepsilon_x]$, (c) $\mathrm{Im}[\varepsilon_z]$, and (d) $\mathrm{Re}[\varepsilon_x]$ with respect to different material parameters of the metal ε_{M}. Dashed lines in (b) correspond to $\mathrm{Im}[\varepsilon_x] = 0.2$.

metallic materials may also compromise and limit our choices and the corresponding collimation effect of the wire medium.

In contrast, we also numerically studied the wire medium in the parallel-stack configuration [shown in Fig. 2(c)] by setting $\varepsilon_{\mathrm{M}} = -5 + 0.5i$ but varying ε_{D}, and the results are presented in Fig. 10, which provides us clear guidance for the choice of appropriate dielectric matrix material by balancing the requirements of small $\mathrm{Im}[\varepsilon_x]$ [below 0.2 within the area of the white dashed line in Fig. 10(b)], large $\mathrm{Im}[\varepsilon_z]$ [bottom left corner in Fig. 10(c)], and a moderate value of the filling ratio f [see Fig. 10(a)].

Using the numerical results in Figs. 9 and 10, we choose AZO ($\varepsilon_{\mathrm{M}} \approx -2 + 0.5i$ at around $\lambda = 1.5$ μm [43,44]) for the wires, which are embedded in a dielectric matrix with $\varepsilon_{\mathrm{D}} = 2 + 0.01i$ in the format of a parallel stack. From Eqs. (18) and (19), we set the radius of the AZO wires to 20 nm, and the lattice constant $a = 100$ nm, so λ/a reaches 15. The calculated $\varepsilon_z \approx 4.7 \times 10^{-3} + 2.26i$, and $\varepsilon_x \approx 1.50 + 0.07i$. We show the results of our full-wave simulations for the designed wire medium and its effective medium equivalence in Figs. 11(b) and 11(a), respectively. A similar beam collimation effect is demonstrated for both cases. The beam propagates with fairly low decay inside the anisotropic medium due to the small value of $\mathrm{Im}[\varepsilon_x]$. On the other hand, a small $\mathrm{Im}[\varepsilon_z]$ of only 2.26 leads to the broadening tendency of the collimated beam in the propagation.

Finally, we would like to discuss the possibility of realizing the lossy zero-$\mathrm{Re}[\varepsilon_z]$ anisotropic material with the so-called perpendicular configuration of the wire medium, as shown in Fig. 2(d). In the scope of the effective medium, ε_x and ε_z of the wire medium will have the following forms [42]:

$$\varepsilon_z = \varepsilon_{//} = f\varepsilon_{\mathrm{M}} + (1 - f)\varepsilon_{\mathrm{D}} \tag{20}$$

and

$$\varepsilon_x = \varepsilon_{\perp} = \varepsilon_{\mathrm{D}} \frac{(1 + f)\varepsilon_{\mathrm{M}} + (1 - f)\varepsilon_{\mathrm{D}}}{(1 - f)\varepsilon_{\mathrm{M}} + (1 + f)\varepsilon_{\mathrm{D}}}. \tag{21}$$

From Eq. (21), the condition of zero $\mathrm{Re}[\varepsilon_z]$ can give us the required filling ratio of the wires f:

$$f = \frac{\varepsilon_{\mathrm{D}}^{\mathrm{R}}}{\varepsilon_{\mathrm{D}}^{\mathrm{R}} - \varepsilon_{\mathrm{M}}^{\mathrm{R}}}. \tag{22}$$

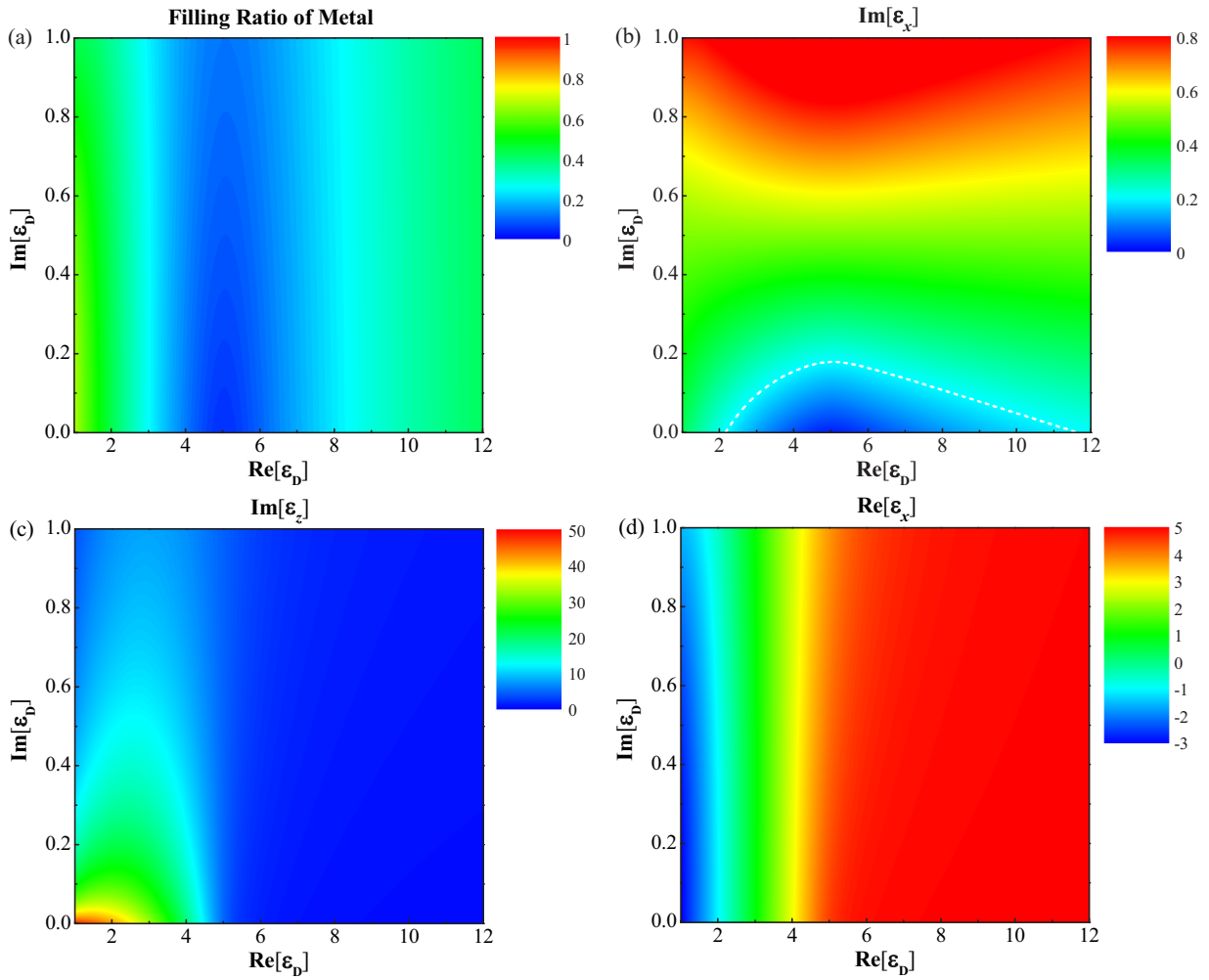

FIG. 10. The case of wire medium under configuration I with $\varepsilon_{\mathrm{M}} = -5 + 0.5i$: Dependence of (a) filling ratio of metal for $\mathrm{Re}[\varepsilon_z] = 0$, (b) $\mathrm{Im}[\varepsilon_x]$, (c) $\mathrm{Im}[\varepsilon_z]$ and (d) $\mathrm{Re}[\varepsilon_x]$ with respect to different material parameters of the dielectric (ε_{D}). Dashed lines in (b) correspond to $\mathrm{Im}[\varepsilon_x] = 0.2$.

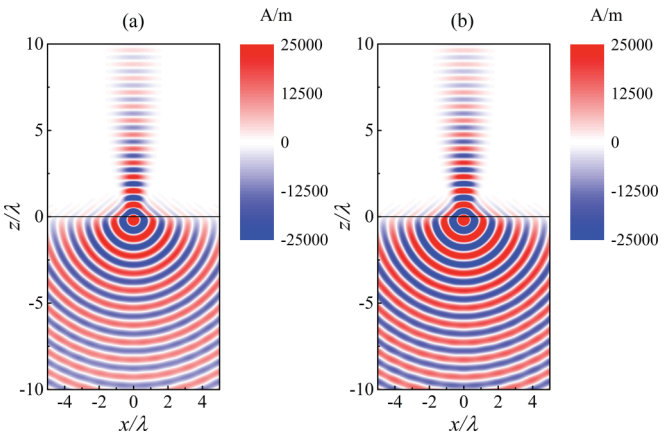

FIG. 11. y component of magnetic field, i.e., H_y for a wire medium at $\lambda = 1.5$ μm (frequency 200 THz) under configuration I: (a) Homogeneous effective medium equivalence and (b) realistic layered structure. Metal wires are 20-nm-radius AZO with $\varepsilon_{\mathrm{M}} = -2 + 0.5i$ embedded in dielectric with $\varepsilon_{\mathrm{D}} = 2 + 0.01i$ and a lattice constant of 100 nm.

With Eqs. (21) and (22), we will easily get the expression for $\mathrm{Im}[\varepsilon_z]$ in the form of ε_{M} and ε_{D},

$$\mathrm{Im}[\varepsilon_z] = \frac{\varepsilon_{\mathrm{D}}^{\mathrm{R}}\varepsilon_{\mathrm{M}}^{\mathrm{I}} - \varepsilon_{\mathrm{M}}^{\mathrm{R}}\varepsilon_{\mathrm{D}}^{\mathrm{I}}}{\varepsilon_{\mathrm{D}}^{\mathrm{R}} - \varepsilon_{\mathrm{M}}^{\mathrm{R}}}. \tag{23}$$

Due to the complexity of Eq. (21), there is no simple expression for $\mathrm{Im}[\varepsilon_x]$ or $\mathrm{Re}[\varepsilon_x]$. Therefore, just like for the other configuration of the wire medium, it will be more intuitive and straightforward to numerically investigate the dependence of $\mathrm{Im}[\varepsilon_x]$ and $\mathrm{Re}[\varepsilon_x]$ on the properties of metallic wires ε_{M} and the dielectric matrix material ε_{D}, as well as the dependence of f and $\mathrm{Im}[\varepsilon_z]$. Then, we can choose the appropriate materials to construct the wire medium accordingly. Two sets of numerical results are presented in Figs. 12 and 13, which correspond to the cases with different ε_{M} with a preset $\varepsilon_{\mathrm{D}} = 5 + 0.01i$ (Fig. 12) and different ε_{D} with a fixed $\varepsilon_{\mathrm{M}} = -100 + 100i$ for a hypothetic metallic material (Fig. 13). In both figures, the dashed line again separates the areas of $\mathrm{Im}[\varepsilon_z] < 0.2$ and $\mathrm{Im}[\varepsilon_z] > 0.2$, so we can first set the preferred regime of the materials to avoid any severe decay of the collimated beam inside the wire medium. According to Fig. 12(c) or Fig. 13(c),

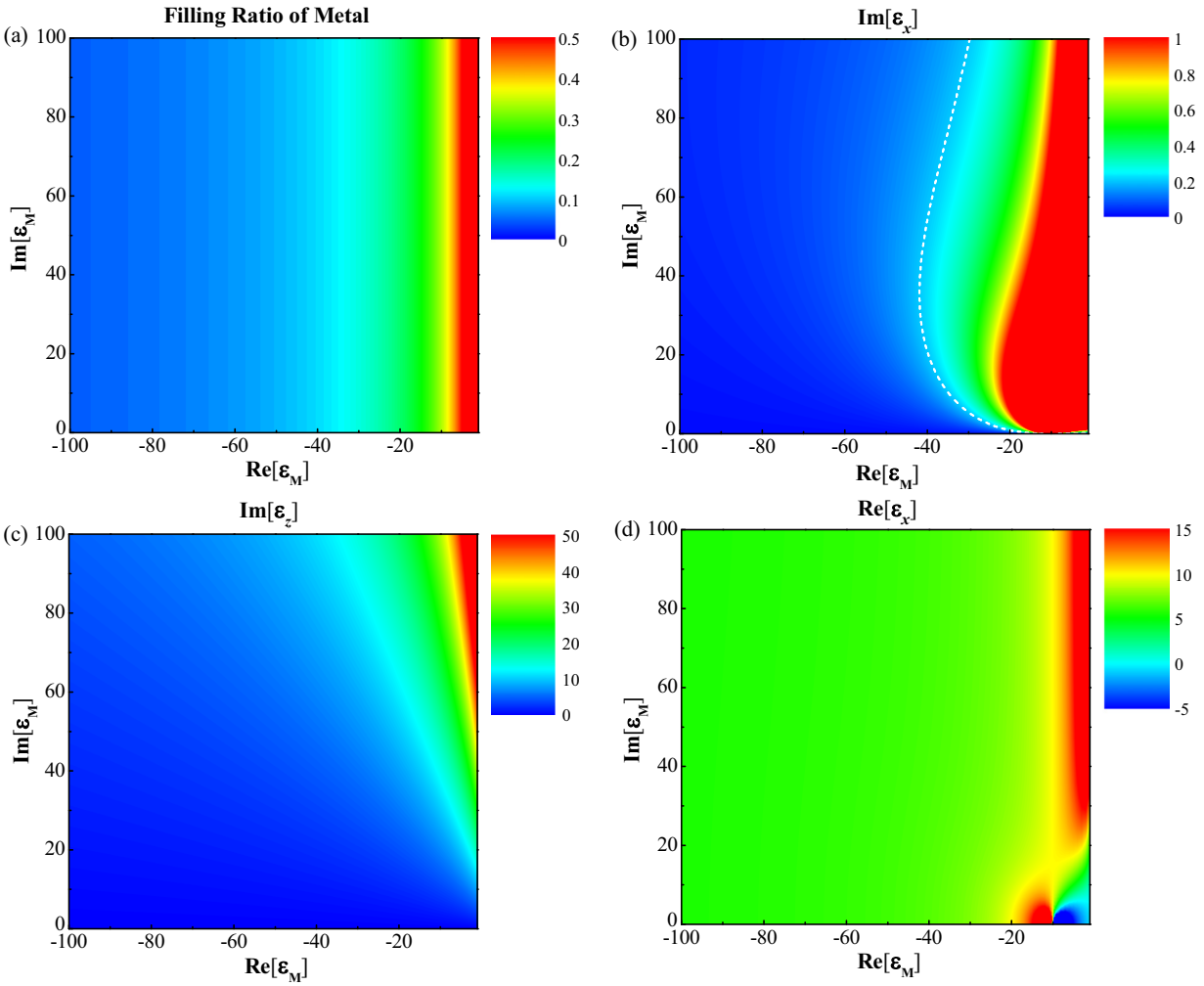

FIG. 12. The case of a wire medium under configuration II with $\varepsilon_D = 5 + 0.01i$: Dependence of (a) the filling ratio of metal for $\mathrm{Re}[\varepsilon_z] = 0$, (b) $\mathrm{Im}[\varepsilon_x]$, (c) $\mathrm{Im}[\varepsilon_z]$, and (d) $\mathrm{Re}[\varepsilon_x]$ with respect to different material parameters of the metal ε_M. The dashed line in (b) corresponds to $\mathrm{Im}[\varepsilon_x] = 0.2$.

we clearly see the tendency in the change of $\mathrm{Im}[\varepsilon_z]$ for different ε_M or ε_D, and therefore, we know what materials to pursue for the large $\mathrm{Im}[\varepsilon_z]$ necessary for a satisfying collimation effect. Like for all the other cases above, we also need to take into account the corresponding filling ratio f, which needs to not make the potential experiments too challenging. All these requirements have to be considered simultaneously to get an acceptable choice of materials to construct the expected wire medium.

According to Figs. 12 and 13, ZrN, which has $\varepsilon_M \approx -172.73 + 196.92i$ at $\lambda = 3$ μm [44], is again a good option for the metallic wires perpendicularly embedded in the dielectric matrix with ε_D set to be $6 + 0.001i$. The lattice constant is 200 nm, with the corresponding $\lambda/a = 15$. From Eq. (23), we find the required radius of the ZrN wires is about 20.7 nm. The calculated $\varepsilon_z \approx -0.01 + 6.63i$ and $\varepsilon_x \approx 6.43 + 0.02i$ from Eqs. (20) and (21). The corresponding full-wave simulation results, i.e., the distribution of the y component of the magnetic field for a magnetic line source in the vacuum in front of the anisotropic medium, can be found in Fig. 14 with both the homogeneous effective medium [Fig. 14(a)] and the realistic wire medium [Fig. 14(b)] applied. As expected, the designed wire medium again gets the incident beams beautifully collimated with fairly low decay in propagation.

So far, we have systematically explored the realization of a high-loss ENZ anisotropic medium with both layered structures and the wire medium. Through the full-wave simulations, we successfully demonstrated loss-induced transmission enhancement at the interface of the ENZ anisotropic medium and the effect of energy collimation for each properly designed configuration. Considering the beam collimation effect associated with EFCs as shown in Fig. 1(d), we need to point out it is not necessary to strictly have zero $\mathrm{Re}[\varepsilon_z]$ if $|\varepsilon_z|$ can be very large, according to Eqs. (2) and (3). Practically, in the presented configurations of a high-loss anisotropic ENZ medium, $|\varepsilon_z|$ has a finite value in general, and nonzero $\mathrm{Re}[\varepsilon_z]$ may lead to the distortion of the flat EFCs, which hurts the expected energy collimation effect. However, the allowed moderate relaxation to the requirement of zero $\mathrm{Re}[\varepsilon_z]$ provides some flexibility in the recipe for constructing an anisotropic medium, and on the other hand, for a designed metamaterial structure, the energy collimation effect may survive within some range of frequencies, which will be greatly beneficial for practical applications.

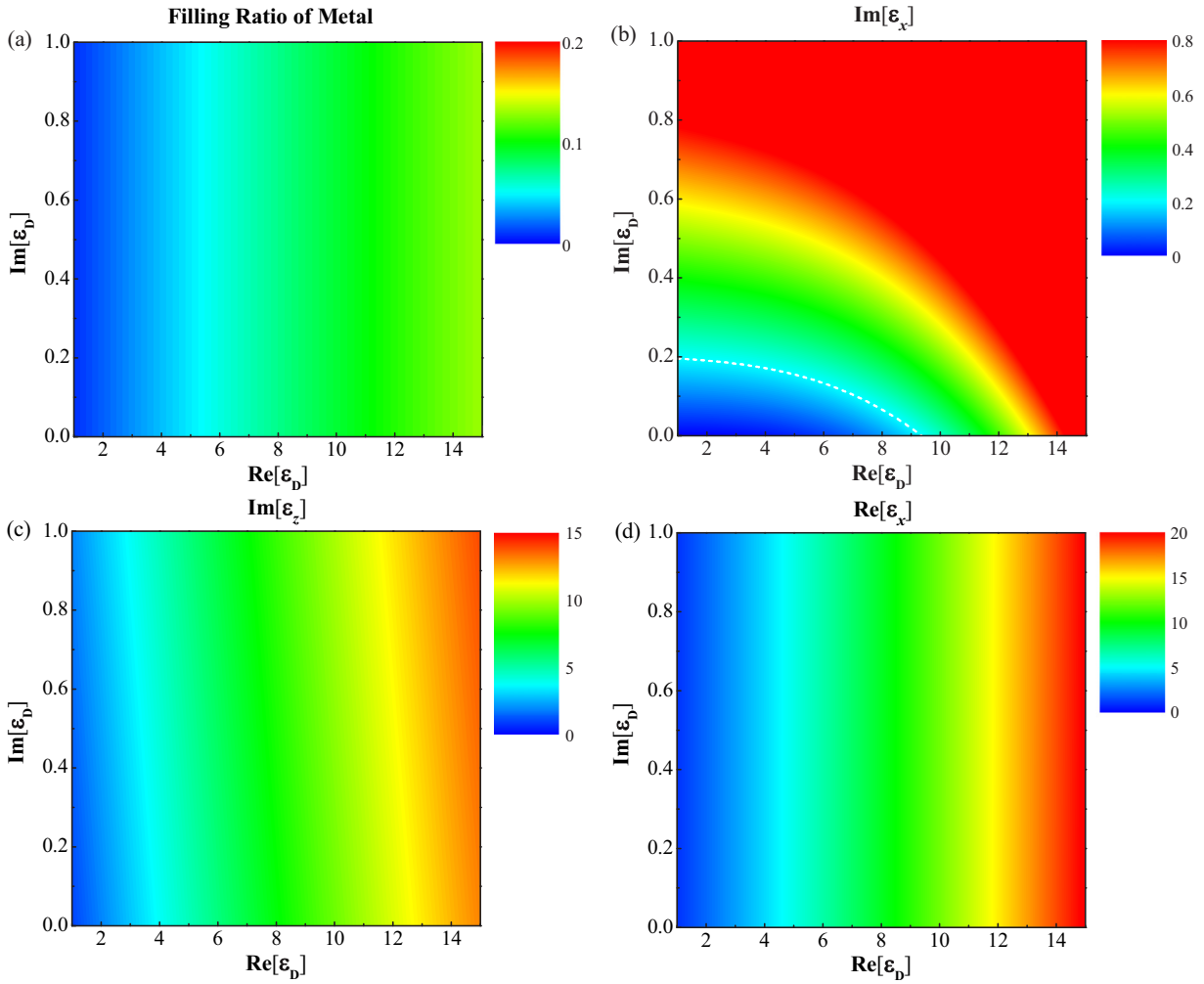

FIG. 13. The case of a wire medium under configuration I with $\varepsilon_{\mathrm{M}} = -100 + 100i$: Dependence of (a) the filling ratio of metal for $\mathrm{Re}[\varepsilon_z] = 0$, (b) $\mathrm{Im}[\varepsilon_x]$, (c) $\mathrm{Im}[\varepsilon_z]$, and (d) $\mathrm{Re}[\varepsilon_x]$ with respect to different material parameters of the dielectric ε_{D}. The dashed line in (b) corresponds to $\mathrm{Im}[\varepsilon_x] = 0.2$.

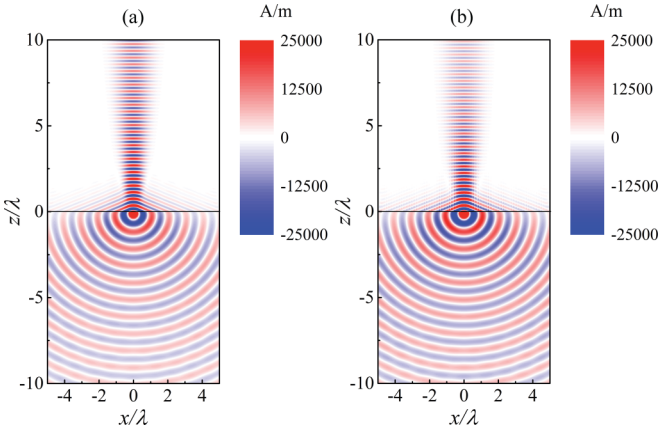

FIG. 14. y component of magnetic field, i.e., H_y for a wire medium at $\lambda = 3\ \mu$m (frequency 100 THz) under configuration II: (a) Homogeneous effective medium equivalence and (b) realistic layered structure. Metal wires are 20.7-nm-radius ZrN with $\varepsilon_{\mathrm{M}} = -172.73 + 196.92i$ embedded in the dielectric with $\varepsilon_{\mathrm{D}} = 6 + 0.001i$ and a lattice constant of 200 nm.

III. CONCLUSIONS

In conclusion, in the scope of effective medium theory, we pursued the possibilities of using metamaterials to realize the special category of a lossy zero-$\mathrm{Re}[\varepsilon_z]$ anisotropic medium, which shows a counterintuitive effect of energy collimation. We systematically investigated the two simplest metamaterial structures of metal-dielectric-layered stacks and the wire medium under both parallel and perpendicular configurations and provided the corresponding recipes for constructing the proposed lossy zero-$\mathrm{Re}[\varepsilon_z]$ anisotropic medium via analytical derivations and numerical simulations. As examples, we designed the metamaterial structure with practical ingredient materials for each configuration and performed full-wave simulations corresponding to them as well as to their effective medium equivalences. We demonstrated a beautiful energy collimation effect for all the example cases, and the results are in excellent agreement for the realistic metamaterial and effective medium. Therefore, our current work provides clear guidance for searching for proper metamaterial designs for a lossy zero-$\mathrm{Re}[\varepsilon_z]$ anisotropic medium and thus paves the way

towards energy harvesting and wave-front manipulation under such a fabulous strategy.

ACKNOWLEDGMENTS

Work at Ames Laboratory was partially supported by the U.S. Department of Energy, Office of Basic Energy Science, Division of Materials Sciences and Engineering (Ames Laboratory is operated for the U.S. Department of Energy by Iowa State University under Contract No. DE-AC02-07CH11358), and by the U.S. Office of Naval Research, Award No. N00014-16-1-2294 (simulations). The European Research Council under ERC Advanced Grant No. 320081 (PHOTOMETA) supported work (theory) at FORTH.

[1] C. M. Soukoulis and M. Wegener, Nat. Photonics **5**, 523 (2011).
[2] N. I. Zheludev and Y. S. Kivshar, Nat. Mater. **11**, 917 (2012).
[3] H. Chen, C. T. Chen, and P. Sheng, Nat. Mater. **9**, 387 (2010).
[4] Y. Liu and X. Zhang, Chem. Soc. Rev. **40**, 2494 (2011).
[5] R. A. Shelby, D. R. Smith, and S. Schultz, Science **292**, 77 (2001).
[6] J. Valentine, S. Zhang, Th. Zentgraf, E. Ulin-Avila, D. A. Genov, G. Bartal, and X. Zhang, Nature (London) **455**, 376 (2008).
[7] J. B. Pendry, Phys. Rev. Lett. **85**, 3966 (2000).
[8] N. Fang, H. Lee, C. Sun, and X. Zhang, Science **308**, 534 (2005).
[9] Z. Liu, H. Lee, Y. Xiong, C. Sun, and X. Zhang, Science **315**, 1686 (2007).
[10] D. Lu and Z. Liu, Nat. Commun. **3**, 1205 (2012).
[11] J. B. Pendry, D. Schurig, and D. R. Smith, Science **312**, 1780 (2006).
[12] D. Schurig, J. J. Mock, B. J. Justice, S. A. Cummer, A. F. Starr, and D. R. Smith, Science **314**, 977 (2006).
[13] L. H. Gabrielli, J. Cardenas, C. B. Poitras, and M. Lipson, Nat. Photonics **3**, 461 (2009).
[14] J. Valentine, J. Li, Th. Zentgraf, G. Bartal, and X. Zhang, Nat. Mater. **8**, 568 (2009).
[15] N. Yu, P. Genevet, M. A. Kats, F. Aieta, J.-P. Tetienne, F. Capasso, and Z. Gaburro, Science **334**, 333 (2011).
[16] A. V. Kildishev, A. Boltasseva, and V. M. Shalaev, Science **339**, 1232009 (2013).
[17] N. Yu and F. Capasso, Nat. Mater. **13**, 139 (2014).
[18] R. W. Ziolkowski, Phys. Rev. E **70**, 046608 (2004).
[19] P. Moitra, Y. Yang, Z. Anderson, I. I. Kravchenko, D. P. Briggs, and J. Valtentine, Nat. Photonics **7**, 791 (2013).
[20] Y. Li, S. Kita, P. Munoz, O. Reshef, D. I. Vulis, M. Yin, M. Loncar, and E. Mazur, Nat. Photonics **9**, 738 (2015).
[21] S. Enoch, G. Tayeb, P. Sabouroux, N. Guerin, and P. Vincent, Phys. Rev. Lett. **89**, 213902 (2002).
[22] Q. Cheng, W. X. Jiang, and T. J. Cui, Phys. Rev. Lett. **108**, 213903 (2012).
[23] M. Silveirinha and N. Engheta, Phys. Rev. Lett. **97**, 157403 (2006).
[24] R. Liu, Q. Cheng, T. Hand, J. J. Mock, T. J. Cui, S. A. Cummer, and D. R. Smith, Phys. Rev. Lett. **100**, 023903 (2008).
[25] V. C. Nguyen, L. Chen, and K. Halterman, Phys. Rev. Lett. **105**, 233908 (2010).
[26] X. Q. Huang, Y. Lai, Z. H. Hang, H. Zheng, and C. T. Chan, Nat. Mater. **10**, 582 (2011).
[27] J. Luo, W. X. Lu, Z. H. Hang, H. Y. Chen, B. Hou, Y. Lai, and C. T. Chan, Phys. Rev. Lett. **112**, 073903 (2014).
[28] Q. Zhao, Z. Xiao, F. Zhang, J. Ma, M. Qiao, Y. Meng, C. Lan, B. Li, J. Zhou, P. Zhang, N.-H. Shen, Th. Koschny, and C. M. Soukoulis, Adv. Mater. **27**, 6187 (2015).
[29] C. M. Soukoulis, S. Linden, and M. Wegener, Science **315**, 47 (2007).
[30] A. Fang, Th. Koschny, M. Wegener, and C. M. Soukoulis, Phys. Rev. B **79**, 241104(R) (2009).
[31] S. Xiao, V. P. Drachev, A. V. Kildishev, X. Ni, U. K. Chettiar, H.-K. Yuan, and V. M. Shalaev, Nat. Mater. **466**, 735 (2010).
[32] O. Hess, J. B. Pendry, S. A. Maier, R. F. Oulton, J. M. Hamm, and K. L. Tsakmakidis, Nat. Mater. **11**, 573 (2012).
[33] N. I. Landy, S. Sajuyigbe, J. J. Mock, D. R. Smith, and W. J. Padilla, Phys. Rev. Lett. **100**, 207402 (2008).
[34] S. Feng, Phys. Rev. Lett. **108**, 193904 (2012).
[35] S. A. Ramakrishna, J. B. Pendry, M. C. K. Wiltshire, and W. J. Stewart, J. Mod. Opt. **50**, 1419 (2002).
[36] P. A. Belov and Y. Hao, Phys. Rev. B **73**, 113110 (2006).
[37] P. A. Belov, Y. Hao, and S. Sudhakaran, Phys. Rev. B **73**, 033108 (2006).
[38] M. G. Silveirinha, P. A. Belov, and C. R. Simovski, Phys. Rev. B **75**, 035108 (2007).
[39] M. G. Silveirinha and N. Engheta, Phys. Rev. B **85**, 085116 (2012).
[40] L. Sun, S. Feng, and X. D. Yang, Appl. Phys. Lett. **101**, 241101 (2012).
[41] H. Jiang, W. Liu, K. Yu, K. Fang, Y. Sun, Y. Li, and H. Chen, Phys. Rev. B **91**, 045302 (2015).
[42] T. C. Choy, *Effective Medium Theory: Principles and Applications* (Oxford University Press, Oxford, 1999).
[43] G. V. Naik, J. Liu, A. V. Kildishev, V. M. Shalaev, and A. Boltasseva, Proc. Natl. Acad. Sci. USA **109**, 8834 (2012).
[44] G. V. Naik, V. M. Shalaev, and A. Boltasseva, Adv. Mater. **25**, 3264 (2013).
[45] J. Yao, Z. Liu, Y. Liu, Y. Wang, C. Sun, G. Bartal, A. M. Stacy, and X. Zhang, Science **321**, 930 (2008).
[46] Y. Liu, G. Bartal, and X. Zhang, Opt. Express **16**, 15439 (2008).
[47] A. Fang, Th. Koschny, and C. M. Soukoulis, Phys. Rev. B **79**, 245127 (2009).
[48] J. Yao, X. Yang, X. Yin, G. Bartal, and X. Zhang, Proc. Natl. Acad. Sci. USA **108**, 11327 (2011).